Excess-entropy scaling of dynamics for a confined fluid of dumbbell-shaped particles

Ravi Chopra,[1,*] Thomas M. Truskett,[2,†] and Jeffrey R. Errington[1,‡]
[1]*Department of Chemical and Biological Engineering, University at Buffalo, The State University of New York, Buffalo, New York 14260, USA*
[2]*Department of Chemical Engineering and Institute for Theoretical Chemistry, University of Texas at Austin, Austin, Texas 78712, USA*
(Received 9 August 2010; published 4 October 2010)

We use molecular simulation to study the ability of excess entropy scaling relationships to describe the kinetic properties of a confined molecular system. We examine a model for a confined fluid consisting of dumbbell-shaped molecules that interact with atomistically detailed pore walls via a Lennard-Jones potential. We obtain kinetic, thermodynamic, and structural properties of the system at three wall-fluid interaction strengths and over a temperature range that includes sub- and super-critical conditions. Four dynamic properties are considered: translational and rotational diffusivities, a characteristic relaxation time for rotational motion, and a collective relaxation time stemming from analysis of the coherent intermediate scattering function. We carefully consider the reference state used to define the excess entropy of a confined fluid. Three ideal-gas reference states are considered, with the cases differentiated by the extent to which one-body spatial and orientational correlations are accounted for in the reference state. Our results indicate that a version of the excess entropy that includes information related to the one-body correlations in a confined fluid serves as the best scaling variable for dynamic properties. When adopting such a definition for the reference state, to a very good approximation, bulk and confined data for a specified dynamic property at a given temperature collapse onto a common curve when plotted against the excess entropy.

DOI: 10.1103/PhysRevE.82.041201 PACS number(s): 66.10.cg, 64.70.qd, 68.08.De, 61.20.Ja

I. INTRODUCTION

Confined fluids feature prominently in both nature and technology. Examples include gases within membrane-based separation devices, water passing through ion channels, liquids in nanofluidic devices, and light gases in nanostructured storage materials (e.g., decorated carbon nanotubes). The behavior of fluids confined to such restricted environments can differ significantly from the bulk. As a result, predicting the influence of confinement on thermodynamic and transport properties can be a challenging task. From an engineering perspective, these properties are important for the efficient design of devices. Recent studies suggest that excess entropy scaling [1–6] serves as a valuable tool for predicting the transport properties of confined fluids [7–13]. At their most basic level, these scaling relationships establish a link between thermodynamic and kinetic properties of this important class of systems, thereby providing a means to predict one based upon knowledge of the other. Investigations focused on the effectiveness of this tool for describing the properties of confined fluids have thus far been limited to models with particles that interact with one another via simple, spherically-symmetric (e.g., atomistic) pair potentials [7–13]. In this work, we move toward an examination of confined fluids of particles with intramolecular degrees of freedom (e.g., molecular fluids) by studying the ability of excess entropy scaling relations to capture the influence of confinement on the kinetic properties of a model fluid consisting of dumbbell-shaped particles.

Mittal *et al.* first examined the prospects of using excess entropy scaling to describe the dynamics of confined fluids [7]. They found that the relationship between self-diffusivity and excess entropy for a collection of hard spherical particles does not change substantially upon confinement of the fluid within a slit pore. While both self diffusivity and excess entropy were found to vary considerably with degree of confinement (i.e., the distance between the confining boundaries), the relationship between the two quantities remained approximately unchanged from that of the bulk fluid. They recognized that establishment of this strong empirical correlation afforded a means to estimate the variation in diffusivity upon confinement when provided information regarding how the excess entropy changes with degree of confinement, and vice versa. Subsequent studies [8–13] focused on monatomic particles governed by a variety of interaction potentials (e.g., hard-sphere, square-well, Lennard-Jones) confined within various restrictive geometries (e.g., rectangular channel, cylindrical pore, strongly attractive walls, weakly attractive walls) all pointed to the same conclusion: to a good approximation, upon confinement a fluid shows the same relationship between diffusivity and excess entropy as the bulk system at the specified temperature.

Excess-entropy scaling strategies have also been examined recently within the context of molecular fluids [14–22]. Such fluids differ from atomistic systems in that they possess rotational and intramolecular degrees of freedom. Initial studies focused on identifying the most relevant scaling variable for these systems. Given the additional relaxation modes available to molecular fluids, one might question whether a transport property associated with a particular type of motion (e.g., translational self-diffusivity) scales with the component of the excess entropy related to the intermolecular correlations associated with those degrees of freedom (e.g., contribution to the excess entropy related to center-of-mass corre-

*rchopra2@buffalo.edu
†truskett@che.utexas.edu
‡jerring@buffalo.edu

lations) or with the total (thermodynamic) excess entropy. A number of studies [14–22] now provide substantial evidence to suggest that the thermodynamic excess entropy correlates strongest with kinetic properties. For example, we have examined the connections between several dynamic properties and various measures of the excess entropy for a Lennard-Jones dumbbell model [22]. We found that the translational self-diffusivity, a collective relaxation time, and two measures of rotational mobility all correlate strongly with the thermodynamic excess entropy over a wide range of state conditions. Although contributions to the two-body excess entropy associated with translational and orientational correlations provided a reasonable description of the dynamic properties in some cases, the thermodynamic excess entropy proved to be the most effective scaling variable for all of the aforementioned kinetic properties considered. Finally, we note that identification of the total excess entropy, a well-defined and relatively accessible thermodynamic quantity, as the optimal scaling variable enhances the attractiveness of entropy scaling as a tool for predicting dynamic quantities.

In this work, we study the connection between kinetic properties and the thermodynamic excess entropy for a confined dumbbell system. More specifically, we investigate the aforementioned Lennard-Jones dumbbell model within a slit pore defined by atomistically detailed substrates. We consider two pore widths and three substrate-fluid interaction strengths that span from a weak to a strong wall potential relative to the fluid-fluid interaction. Four dynamic quantities are examined: the translational diffusion coefficient, the rotational diffusion coefficient, a relaxation time for rotational motion, and a collective relaxation time. We first examine issues related to the reference state used to define the excess entropy. Our analysis focuses on how one-body correlations should be managed. We find that a version of excess entropy that includes information related to one-body correlations within the confined fluid best captures the trends in the dynamics. When adopting such a definition for the reference state, to a very good approximation, bulk and confined data for a specified dynamic property at a given temperature collapse onto a common curve when plotted against the thermodynamic excess entropy. The calculations performed here suggest that excess entropy scaling provides a convenient means to capture the influence of confinement on the dynamic properties of simple molecular fluids.

The paper is organized as follows. In the following sections we describe the model examined in this work and the molecular simulation methods used to compute thermodynamic, structural, and kinetic properties of interest. Next, we examine the sensitivity of excess entropy scaling strategies to the choice for the reference state used to define excess functions. Finally, we consider the feasibility of using excess entropy scaling to describe the effect of confinement on a wide range of kinetic properties.

II. MOLECULAR MODEL

The model system consists of a fluid of dumbbell-shaped particles that interact with each other and with two parallel, static atomistically detailed substrates via a truncated Lennard-Jones potential. The energy of interaction u_{ij} between any two nonbonded interaction sites separated by a distance r is given by

$$u_{ij}(r) = \begin{cases} u_{ij}^{\mathrm{LJ}}(r_{ij}) & \text{for } r < r_{ij}^{\mathrm{c}} \\ 0 & \text{for } r > r_{ij}^{\mathrm{c}} \end{cases}, \tag{1}$$

with

$$u_{ij}^{\mathrm{LJ}}(r) = 4\varepsilon_{ij}\left[\left(\frac{\sigma_{ij}}{r}\right)^{12} - \left(\frac{\sigma_{ij}}{r}\right)^{6}\right], \tag{2}$$

where ε_{ij} and σ_{ij} are energy and size parameters, respectively. The fluid-fluid (ff) and substrate-fluid (sf) interactions are cutoff at distances of $r_{\mathrm{ff}}^{\mathrm{c}}=r_{\mathrm{sf}}^{\mathrm{c}}=2.5\sigma_{\mathrm{ff}}$. The characteristic length scales of the ff and sf interactions are identical, $\sigma_{\mathrm{sf}}=\sigma_{\mathrm{ff}}$. We work with characteristic energy scales of $\varepsilon_{\mathrm{sf}}/\varepsilon_{\mathrm{ff}}=0.2$, 1.0, and 3.0, which we refer to as weak, moderate and strong wall strengths, respectively. Substrate particles are arranged in an fcc lattice with a density of $\rho=1.4142\sigma_{\mathrm{ff}}^{-3}$ and the (100) plane is exposed to the fluid. The slit pore consists of a lower substrate with the centers of particles within the top layer positioned at $z=0$ and an upper substrate with the centers of particles within the bottom layer positioned at $z=H$. The top layer of the lower substrate and the bottom layer of the upper substrate are aligned laterally (i.e., the substrates are in registry with one another). We work with a dumbbell molecule that contains interaction sites separated by a distance $L=\sigma_{\mathrm{ff}}$ and consider two slit pores with $H=5\sigma_{\mathrm{ff}}$ and $10\sigma_{\mathrm{ff}}$. In what follows, all quantities are made dimensionless using the characteristic energy and length scales of the fluid-fluid interaction. For example, temperature is reduced by $\varepsilon_{\mathrm{ff}}/k$ (k is Boltzmann's constant), distance by σ_{ff}, entropy by k, and time by $\sqrt{m\sigma_{\mathrm{ff}}^2/\varepsilon_{\mathrm{ff}}}$, where m is the mass of a dumbbell molecule, which is set to unity in this work.

III. COMPUTATIONAL METHODS

A. Excess entropy

To calculate the excess entropy we first employ Monte Carlo simulation to determine the entropy of a fluid containing N particles within a confined environment at temperature T [7,23]. We then use information related to the structure of this simulated fluid to compute the entropy of an ideal-gas reference state. The difference between these two quantities is the excess entropy. Simulations are conducted using a rectangular parallelepiped cell with periodic boundary conditions applied in two of the three directions. The cell is closed at each end in the nonperiodic direction with substrates of cross-sectional area A separated by a distance H. We employ a two-step process to determine the entropy at conditions of interest. In the first step we obtain the density-dependence of the entropy at relatively high temperature T_h using grand canonical transition matrix Monte Carlo simulation (GC-TMMC) [24,25]. GC-TMMC simulations are conducted at T_h, volume $V=AH$, and activity $\xi_h=q_h\exp(\beta_h\mu_h)$, where $\beta=1/T$ is the inverse temperature, μ is the chemical potential, and q represents the component of the molecular partition function stemming from integration over momenta. The key quantity extracted from the GC-TMMC simulation is the par-

ticle number probability distribution $\Pi_{GC}(N;\beta_h,\xi_h)$.

In the second step we perform a canonical temperature expanded ensemble transition matrix Monte Carlo simulation (TE-TMMC) to evaluate the change in entropy with temperature at constant density. A canonical temperature expanded ensemble [21,22,26,27] consists of a collection of subensembles that share the same particle number N and volume V while possessing different temperatures. In this work, we take the inverse temperature β as the order parameter and establish a set of subensembles that range from β_{min} to β_{max} in increments of $\Delta\beta$. The key quantities extracted from the TE-TMMC simulation are the inverse temperature probability distribution $\Pi_{TE}(\beta;N)$ and configurational energy $U(\beta,N)$. Collectively, the GC-TMMC and TE-TMMC simulations provide the configurational entropy at a given inverse temperature β and particle number N of interest,

$$S(\beta,N) = \beta U(\beta,N) + \ln\left[\frac{\Pi_{GC}(N;\beta_h,\xi_h)}{\Pi_{GC}(0;\beta_h,\xi_h)}\right] + \ln\left[\frac{\Pi_{TE}(\beta;N)}{\Pi_{TE}(\beta_h;N)}\right] - N\ln\left(\frac{\xi_h}{q}\right). \tag{3}$$

For both the GC- and TE-TMMC simulations we used multicanonical sampling techniques [28] to uniformly sample the density or temperature range of interest.

We now turn our attention toward the reference state used to establish excess functions. In this work, we outline several reasonable choices for the reference state and examine the ability of the associated excess entropies to describe the dynamic properties of a confined fluid. We begin with a commonly used reference system for inhomogeneous fluids: an ideal gas that possesses the same spatial and orientational distribution as the real fluid at the temperature and particle number of interest. This reference state accounts for one-body correlations (single molecule spatial and orientational correlations that stem from the potential field created by the pore walls) within the ideal gas. For a rigid linear molecule the ideal-gas configurational entropy is expressed as [29]

$$S_f^{ig} = -\int d\mathbf{r}d\theta d\phi\rho(\mathbf{r},\theta,\phi)\left\{\ln\left[\frac{4\pi}{q}\rho(\mathbf{r},\theta,\phi)\right]-1\right\}, \tag{4}$$

where $\mathbf{r}$ provides the center of mass position vector, θ is the polar angle defined by the vector connecting the two dumbbell atoms of a molecule and the normal vector of the substrate, ϕ is the azimuthal angle in the plane parallel to the substrates, $\rho(\mathbf{r},\theta,\phi)$ provides the density distribution, and the subscript "f" is used to distinguish this "full" calculation of the ideal-gas configurational entropy from alternative approaches detailed below. To facilitate the entropy calculation, we separate $\rho(\mathbf{r},\theta,\phi)$ into a position-dependent density profile $\rho(\mathbf{r})$ and conditional orientational distribution function $\alpha(\theta,\phi|\mathbf{r})$ [29],

$$\rho(\mathbf{r},\theta,\phi) = \rho(\mathbf{r})\alpha(\theta,\phi|\mathbf{r}), \tag{5}$$

with $\alpha(\theta,\phi|\mathbf{r})$ normalized such that,

$$\int_0^{2\pi} d\phi\int_{-1}^{1} d\cos\theta\,\alpha(\theta,\phi|\mathbf{r}) = 1. \tag{6}$$

We now express S_f^{ig} in terms of a translational contribution S_t^{ig} and an orientational contribution S_o^{ig} [30],

$$S_f^{ig} = S_t^{ig} + S_o^{ig}, \tag{7}$$

with

$$S_t^{ig} = -\int d\mathbf{r}\rho(\mathbf{r})\left\{\ln\left[\frac{\rho(\mathbf{r})}{q}\right]-1\right\}, \tag{8}$$

and,

$$S_o^{ig} = -\int d\mathbf{r}\rho(\mathbf{r})S^{or}(\mathbf{r}), \tag{9}$$

with

$$S^{or}(\mathbf{r}) = \int_0^{2\pi} d\phi\int_{-1}^{1} d\cos\theta\,\alpha(\theta,\phi|\mathbf{r})\ln[4\pi\alpha(\theta,\phi|\mathbf{r})]. \tag{10}$$

Molecular center-of-mass positions and orientations are extracted from configurations taken from canonical Monte Carlo simulations and used to populate a histogram $H(\mathbf{r},\cos\theta,\phi)$. The lateral position of a molecule (x,y) is mapped onto a single unit cell of the fcc crystal. Positions and orientations are discretized with $\Delta x=\Delta y=a/40$, where $a=1.4142$ is the edge length of a fcc unit cell, $\Delta z=0.02$, $\Delta\cos\theta=0.1$, and $\Delta\phi=10°$. Storage requirements are reduced by taking advantage of fourfold symmetry within the 100 face of the fcc crystal, twofold symmetry in the direction normal to the surface, and twofold symmetry in the azimuthal angle ϕ. The conditional distribution function $\alpha(\theta,\phi|\mathbf{r})$ is obtained by normalizing $H(\mathbf{r},\cos\theta,\phi)$ such that Eq. (6) is satisfied. The quantities $S^{or}(\mathbf{r})$, S_o^{ig}, and S_t^{ig} are then computed via numerical integration of Eqs. (8)–(10).

The separation of S_f^{ig} into positional and orientational entropies leads to a second reasonable reference state: an ideal gas that possesses the same center-of-mass spatial distribution as the real fluid at the temperature and particle number of interest, but whose orientational distribution is uniform. The relevant reference state entropy is then S_t^{ig}. This reference state includes one-body correlations associated with the position of the dumbbell center-of-mass only.

The final and simplest reference state that we examine is that of a completely uncorrelated ideal gas that occupies the same volume as, and also has the same temperature and particle number as, the actual simulated confined fluid. This reference state meets the minimal requirement of recognizing the boundaries of the inhomogeneous fluid. One-body spatial and orientational correlations are not accounted for. To determine this accessible volume, we locate a dividing surface via analysis of the laterally averaged segment density profile $\rho_a(z)$ [31]. For each state point, we use $\rho_a(z)$ to deduce an effective surface-fluid interaction potential $\beta u^{eff}(z) = -\ln[\rho_a(z)]$ and subsequently employ a "Boltzmann factor criteria" [32–34] to determine the equivalent hard-core length scale of this effective fluid-particle interaction. To

implement this approach, one first separates the interaction potential $u^{\text{eff}}(z)$ into repulsive $u_0^{\text{eff}}(z)$ and attractive $u_1^{\text{eff}}(z)$ contributions. Here, we use the well-known Weeks-Chandler-Andersen approach [35] to perform this division. The effective hard-core diameter $\sigma_{\text{sf}}^{\text{HS}}$ is then identified using the expression, $\beta u_0^{\text{eff}}(\sigma_{\text{sf}}^{\text{HS}})=c$, where c is a constant typically set between 1 and 2. Based on the success of this approach with $c=1$ to describe effective pore densities in an earlier study [9], we employ this value here as well. The hard-core diameter is used to deduce the effective pore width H^{eff} sampled by fluid molecules. To be consistent with Eq. (4), H^{eff} is obtained by considering the volume accessible to particle centers, which gives $H^{\text{eff}}=H-2\sigma_{\text{sf}}^{\text{HS}}$ [31]. The configurational entropy of the uncorrelated ideal gas is then,

$$S_{\text{u}}^{\text{ig}} = N[\ln(qAH^{\text{eff}}/N) + 1]. \tag{11}$$

Below we examine how the ideal-gas configurational entropies discussed above evolve with temperature, density, and the strength of the substrate. We find it convenient to examine the evolution of these quantities relative to the configurational entropy $S_{\text{V}}^{\text{ig}}=N[\ln(qV/N)+1]$, which corresponds to that of an uncorrelated ideal gas that occupies the volume V defined above. We also study correlations between dynamic properties and various versions of the excess entropy $S_x^{\text{ex}}=S-S_x^{\text{ig}}$, where x is one of f, t, or u.

B. Dynamic properties

We calculate the translational self-diffusivity D_{t} by fitting the long-time behavior of the average mean-squared displacement of the dumbbell center of mass using the Einstein relation [36],

$$\lim_{t\to\infty}\langle|\Delta\vec{r}(t)|^2\rangle = 2dD_{\text{t}}t, \tag{12}$$

where $\Delta\vec{r}(t)=\vec{r}(t)-\vec{r}(0)$ corresponds to the displacement of a center-of-mass at time t in the d periodic directions. We calculate a rotational diffusivity using an approach introduced by Kämmerer *et al.* [37] For a given molecule i, we first define a normalized polarization vector $\hat{p}_i(t)$ using the line connecting the two atom centers of the dumbbell. Next, we define a vector rotational displacement as

$$\vec{\varphi}_i(\Delta t) = \int_t^{t+\Delta t} \Delta\vec{\varphi}_i(t')dt', \tag{13}$$

where $\Delta\vec{\varphi}_i(t')$ is a vector with direction given by $\hat{p}_i(t')\times\hat{p}_i(t'+dt')$ and with magnitude given by $|\Delta\vec{\varphi}_i(t')|=\cos^{-1}[\hat{p}_i(t')\cdot\hat{p}_i(t'+dt')]$. We calculate the rotational diffusivity D_{r} by fitting the long-time behavior of the rotational mean square displacement,

$$\lim_{t\to\infty}\langle|\vec{\varphi}_i(t') - \vec{\varphi}_i(t)|^2\rangle = 4D_{\text{r}}t, \tag{14}$$

where $\vec{\varphi}_i(t')$ and $\vec{\varphi}_i(t)$ are vectors that define a trajectory in three-dimensional space representing the accumulated rotation of dumbbell i at times t' and t, respectively.

To complement the translational and rotational diffusion coefficients we also evaluate a collective relaxation time and dipole relaxation time. The collective relaxation time τ is defined as the time required for the normalized coherent intermediate-scattering function $F(q_0,t)$ to decay to a value of e^{-1}. The wave number q_0 corresponds to the approximate location of the first peak in the structure factor. The dipole relaxation time τ_2 associated with the rotational motion of a dumbbell is defined by the time required for the correlation function $\langle P_2[\cos\theta(t)]\rangle$ to decay to a value of e^{-1}. P_2 is the second Legendre polynomial and $\theta(t)$ is the angle defined by the orientation vectors of a molecule at times t and zero.

C. Simulation details

We performed Monte Carlo (MC) and molecular-dynamics (MD) simulations to acquire thermodynamic, kinetic, and structural data over the range of state conditions defined by $1.0<T<5.0$ and $0.2<\rho=N/V<0.6$. For the MC simulations, we used boxes with interfacial areas of 10×10 and 7×7 square unit cells for the $H=5$ and $H=10$ pores, respectively. These interfacial areas correspond to simulation box volumes of $V=1000$ and 980, respectively. For relatively low densities, we first completed a single GC-TMMC simulation at $T_h=10$ with $\ln\xi_h=0$, and subsequently performed multiple TE-TMMC simulations over the inverse temperature range $T^{-1}=0.1$ to 1.0, with a subensemble spacing of $\Delta T^{-1}=1.0\times10^{-3}$. For relatively high densities, we first completed a single GC-TMMC simulation at $T_h=100$ with $\ln\xi_h=0$, and subsequently performed multiple TE-TMMC simulations over the inverse temperature range $T^{-1}=0.01$ to 1.0. In this latter case, inverse temperature space was separated into two intervals, with one TE-TMMC simulation spanning $T^{-1}=0.01$ to 0.1 with $\Delta T^{-1}=1.0\times10^{-4}$ and the second covering $T^{-1}=0.1$ to 1.0 with $\Delta T^{-1}=1.0\times10^{-3}$.

Molecular dynamics simulations were completed with the GROMACS package [38–41]. We adjusted the number of dumbbell molecules ($N\geq500$) and the size of the fcc lattice structure to obtain a desired density while maintaining periodic boundary conditions. The temperature was controlled using a Nose-Hoover thermostat [42,43] and the system was propagated using the velocity-Verlet method [44,45] with a time step of $\Delta t=2.0\times10^{-3}$. The SHAKE algorithm [46] was used to maintain the dumbbell bond length.

Statistical uncertainties were determined by performing four independent sets of simulations. The standard deviation of the results from the four simulation sets was taken as an estimate of the statistical uncertainty.

IV. RESULTS AND DISCUSSION

We begin by establishing the phase behavior of the dumbbell model. GC-TMMC simulation [24] was used to deduce the bulk liquid-vapor coexistence envelope and saturation conditions at $T=1.0$ for the fluid confined within the various pores studied here. The critical temperature of the bulk fluid is approximately $T_{\text{c}}=1.59$. This estimate was obtained from a curve fit with the scaling relation, $\rho_{\text{l}}-\rho_{\text{v}}\sim(T_{\text{c}}-T)^{\beta}$, where ρ_{l} and ρ_{v} are the saturated liquid and vapor densities, respectively, and $\beta=0.326$ is a scaling exponent. Saturated densities of the bulk and confined fluids at $T=1.0$ are provided in Table I. As is expected for confined fluids [47], the saturated

TABLE I. Liquid-vapor saturation properties at $T=1.0$.

H	ε_{sf}	ρ_v	ρ_l
Bulk		0.001	0.392
5	0.2	0.004	0.265
5	1.0	0.041	0.293
5	3.0	0.227	0.314
10	0.2	0.002	0.319
10	1.0	0.105	0.350
10	3.0	0.194	0.381

densities shift to higher values as the strength of the substrate-fluid interaction increases. We did not use rigorous methods to locate solid-liquid phase diagrams, however, data from TE-TMMC simulations provided insight regarding the location of these curves. The bulk system remained a fluid at temperatures as low as $T=1.0$ for densities as high as $\rho=0.525$. At $\rho=0.550$, 0.575, and 6.0, the bulk system crystallized between $T=1.0$ and 2.0. For both the $H=5$ and 10 pores, the fluid appeared to crystallize between $T=1.0$ and 2.0 at $\rho=0.500$ and between $T=2.0$ and 5.0 at $\rho=0.550$, regardless of substrate strength. Our simulations cover the range from $\rho=0.200$ to the freezing region at $T=2.0$ and 5.0. At $T=1.0$, we examine states beyond the saturated liquid density of the liquid-vapor transition to densities in the vicinity of the freezing transition. In some cases, we suspect that data were collected within the (metastable) supercooled liquid regime, as is common in simulations of dense fluids. Again, accurate information regarding the freezing transition is needed to clarify this issue.

The atomistic-level corrugation of the pore walls coupled with the relatively small size of the pores studied here results in strong spatial and orientational heterogeneities within the fluid structure. Figure 1 shows the laterally averaged spatial density profile $\rho(z)$ at select conditions. Figures 1(a) and 1(b) contrast fluid structure within the $H=10$ and $H=5$ pores. A nearly spatially homogeneous fluid is obtained at the interior of the $H=10$ pore to densities as high as $\rho\approx0.45$, whereas the interior of the $H=5$ pore becomes spatially inhomogeneous at $\rho\approx0.30$. The density profiles presented in Fig. 1(c) suggest that qualitative aspects of the fluid structure do not change significantly with temperature. Increasing temperature simply dampens the strength of the oscillations in $\rho(z)$ while the period of these oscillations remains unchanged. This is suspected for dense fluids of particles whose structural correlations are dominated by the repulsive part of the pair potential. The general shape of $\rho(z)$ also appears to be preserved upon variation of the strength of the substrate-fluid interaction [see Fig. 1(d)]. In this case, the fluid structure closest to the wall is impacted the most, with weaker walls associated with a broader spatial distribution of molecules near the substrate.

Figure 2 shows the lateral density profile $\rho(x,y)$ at $z=0.83$ within the $H=5$ pore with $\varepsilon_{sf}=1.0$, $T=2.0$, and $\rho=0.450$. The vertical distance corresponds to the position at which $\rho(z)$ first reaches a maximum. As a point of reference, the vertical density profile $\rho(z)$ for this system corresponds to

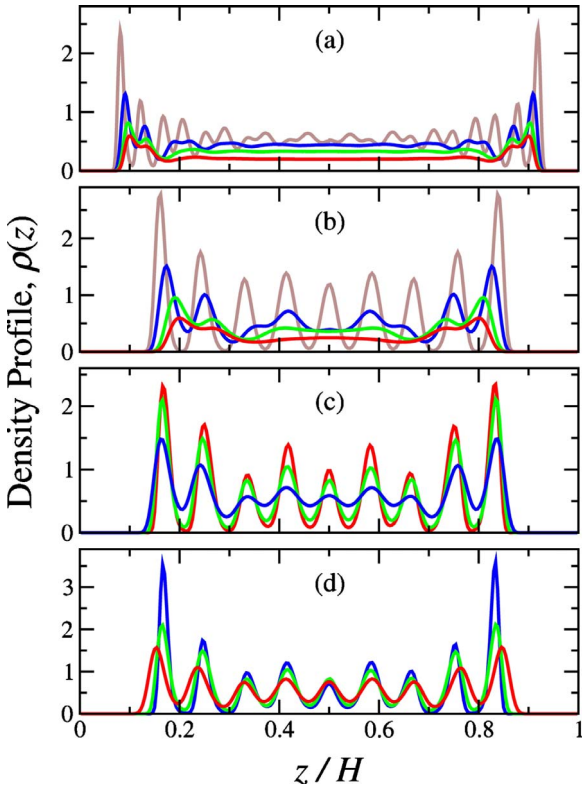

FIG. 1. (Color online) Laterally averaged density profiles $\rho(z)$. (a) $H=10$, $\varepsilon_{sf}=1.0$, and $T=2.0$. Curves from bottom to top (center of the pore) correspond to $\rho=0.2$ (red), 0.3 (green), 0.4 (blue), and 0.5 (brown). (b) $H=5$, $\varepsilon_{sf}=1.0$, and $T=2.0$. Curves from bottom to top (center of the pore) correspond to $\rho=0.2$ (red), 0.3 (green), 0.4 (blue), and 0.5 (brown). (c) $H=5$, $\varepsilon_{sf}=1.0$, and $\rho=0.45$. Curves from bottom to top (center of the pore) correspond to $T=5.0$ (blue), 2.0 (green), and 1.0 (red). (d) $H=5$, $T=2.0$, and $\rho=0.45$. Curves from bottom to top (peaks closest to the wall) correspond to $\varepsilon_{sf}=0.2$ (red), 1.0 (green), and 3.0 (blue).

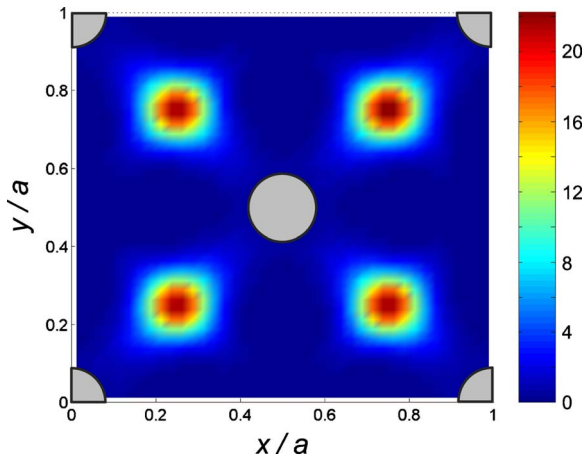

FIG. 2. (Color online) Lateral density profile $\rho(x,y)$ at $z=0.83$ for the $H=5$, $\varepsilon_{sf}=1.0$ pore at $T=2.0$, $\rho=0.45$. The figure spans one square unit cell of the fcc lattice. The gray circle and quarter circles show the location of atoms in the outermost layer of the 100 face of the fcc crystal.

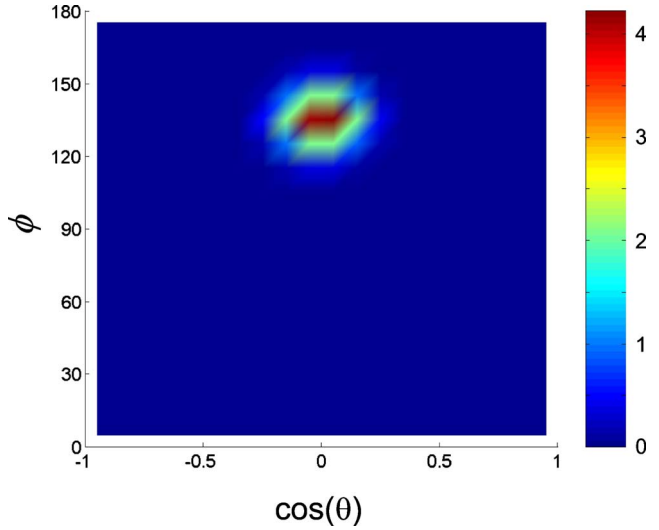

FIG. 3. (Color online) Conditional orientational distribution function $\alpha(\cos\theta,\phi|\mathbf{r})$ at $x/a=y/a=0.25$ and $z=0.83$ for the $H=5$, $\varepsilon_{sf}=1.0$ pore at $T=2.0$, $\rho=0.45$.

the middle (green) curves presented in Figs. 1(c) and 1(d). The profile presented in Fig. 2 spans one square unit cell of the fcc lattice, with the 100 face in contact with the fluid. The distribution is highly localized, with the dumbbell centers of mass preferentially adopting lateral positions corresponding to the midpoints of lines connecting adjacent atoms in the top layer of the fcc lattice. At these positions the vector defined by the dumbbell intramolecular bond lies perpendicular to the substrate normal and perpendicular to the aforementioned vector connecting adjacent atoms in the outermost face of the fcc lattice. In terms of the (θ,ϕ) notation outlined above, the dumbbells adopt orientations characterized by $\cos\theta\approx 0$ and $\phi\approx\pi/4$ or $\phi\approx 3\pi/4$. An example of the conditional orientational distribution function $\alpha(\theta,\phi|\mathbf{r})$ with $x/a=y/a=0.25$ and $z=0.83$ at the same state point noted above is presented in Fig. 3. The spatial position selected corresponds to the location of the maximum in the lower left quadrant of the $\rho(x,y)$ profile shown in Fig. 2. Similar to the $\rho(x,y)$ profile, the $\alpha(\theta,\phi|\mathbf{r})$ distribution is highly localized. The combined center of mass location and dumbbell orientation places the dumbbell atoms at local depressions within the 100 surface of the fcc crystal. This result is intuitively expected. The distributions provided in Figs. 2 and 3 provide quantitative representations of the strength of the one-body dumbbell correlations.

Figure 4 provides ideal-gas configurational entropies for the dumbbell fluid within the $H=5$ and 10 pores with $\varepsilon_{sf}=1.0$ at $T=2.0$. For convenience, we plot the entropy difference $\Delta s_x^{ig}=(S_x^{ig}-S_V^{ig})/N$. As the fluid density increases, the one-body spatial and orientational distributions become progressively more localized and Δs_t^{ig}, Δs_o^{ig}, and Δs_f^{ig} monotonically increase. In contrast, the accessible-volume-based Δs_u^{ig} remains relatively constant with increasing density. For the systems studied here, the orientational contribution Δs_o^{ig} is larger than the translational term Δs_t^{ig} at almost all state conditions. Although it is difficult to appreciate from Fig. 4, Δs_t^{ig} exceeds Δs_o^{ig} at low density, where both quantities are relatively small. The $H=10$ entropy differences Δs_x^{ig} are small

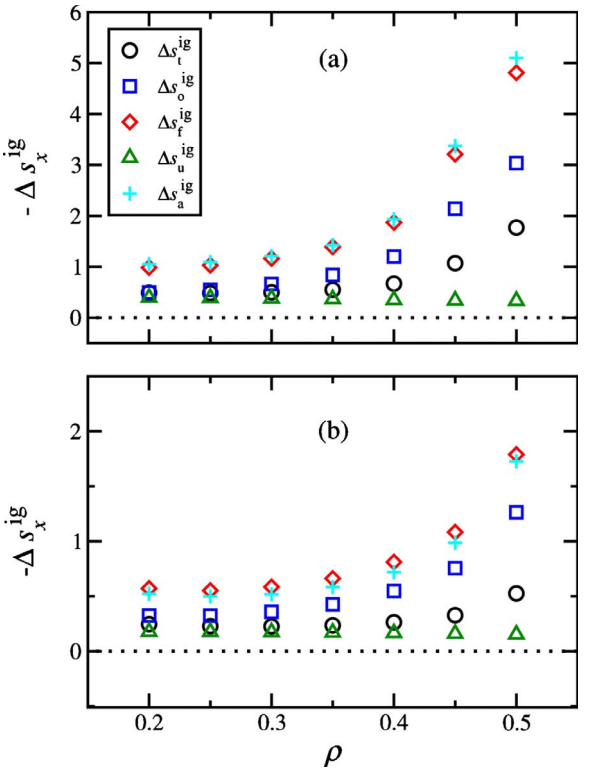

FIG. 4. (Color online) Ideal-gas entropies for the (a) $H=5$ and (b) $H=10$ pores with $\varepsilon_{sf}=1.0$ at $T=2.0$. Symbols represent different versions of the reference state entropy as denoted within the legend.

relative to the $H=5$ values at similar fluid conditions. This result is generally expected; as the surface to volume ratio increases, the fraction of molecules influenced by the pore walls increases, leading to larger one-body entropies on average.

We also include in Fig. 4 results from a segment-based approach for computing the ideal-gas configurational entropy. In this case, one uses the atomic density profiles $\rho_a(\mathbf{r})$ to approximate the total one-body configurational entropy [48–50]. More specifically, the ideal-gas configurational entropy S_a^{ig} stems from a summation of integrals similar to that presented in Eq. (8), but featuring segment densities,

$$S_a^{ig}=-\frac{1}{n}\sum_{j=1}^{n}\int d\mathbf{r}\rho_j(\mathbf{r})\left\{\ln\left[\frac{\rho_j(\mathbf{r})}{q}\right]-1\right\}, \qquad (15)$$

where n is the number of segments within a molecule. Chandler *et al.* explain [49] that this "extended-atom" approach is expected to provide a good approximation to s_f^{ig} for diatomic molecules when the intramolecular bond length becomes large. We find that Δs_a^{ig} tracks Δs_f^{ig} reasonably well, suggesting that the atoms within a given molecule are largely seen as independent entities by surrounding fluid molecules. This result is perhaps not too surprising given the geometry of the dumbbell model studied here.

The strong one-body spatial and orientational correlations within the confined dumbbell fluid result in relatively large differences in the various ideal-gas entropies. It follows that the choice of reference state will have a significant impact on

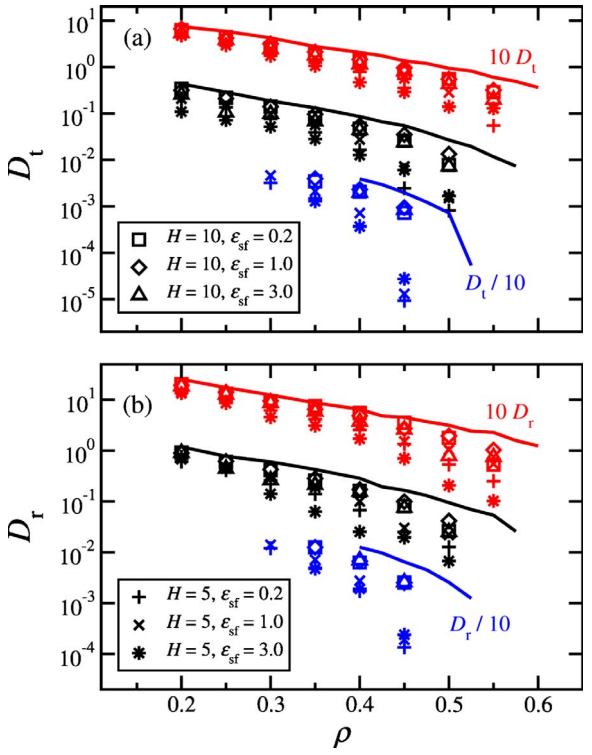

FIG. 5. (Color online) (a) translational and (b) rotational diffusion coefficients. Symbols represent different pore width and wall strength combinations as denoted within the legend. Solid lines represent the bulk fluid. Data are grouped from bottom to top as $T=1.0$ (blue), $T=2.0$ (black), and $T=5.0$ (red).

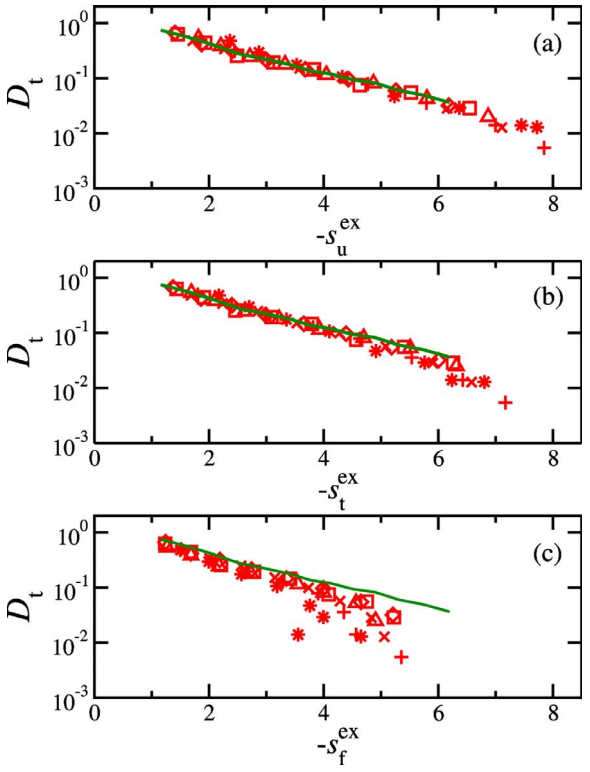

FIG. 6. (Color online) Relationship between translational diffusivity and various versions of the excess entropy at $T=5.0$. Symbol shape is consistent with the definition adopted in Fig. 5. Solid lines represent the bulk fluid.

the quality of excess entropy scaling predictions. Before examining the ability of the candidate excess entropies Δs_x^{ex} to describe the dynamics of the confined dumbbell fluid, we provide some perspective regarding the magnitude of the ideal-gas entropies provided in Fig. 4. All previous applications of excess entropy scaling to confined systems have focused on fluids described by spherically symmetric interaction potentials (e.g., atomistic fluids) within pores defined by smooth structureless walls [7–13]. Such systems are inhomogeneous in the direction normal to the substrate only. As a result, the difference between s_f^{ig} and s_u^{ig} is typically small. A relevant example comes from the study of Mittal *et al.* [7], who examined the hard-sphere fluid confined by smooth hard walls. For a pore width of five fluid diameters, the difference $s_f^{ig}-s_u^{ig}$ evaluates to around −0.35 when the system is in the vicinity of the freezing point. In contrast, this value approaches −5 under similar conditions for the dumbbell system studied here. As we will see below, the relatively large difference between s_f^{ig} and s_u^{ig} for the dumbbell system will help us to clarify the relevant reference state for predicting dynamic properties.

Figure 5 provides the temperature and density dependence of the translational and rotational diffusivities of the bulk and confined dumbbell fluids. As expected, the mobility of the molecules decreases with increasing density and decreasing temperature. We also find that the diffusivities are sensitive to the wall strength, with higher particle mobilities in the pores with weaker walls. This observation indicates that density alone cannot be used to reliably predict the dynamic properties of confined fluids. If one were to consider an effective density based upon the accessible volume, the correlation with dynamic properties would generally improve, but this strategy would help little in terms of collapsing data obtained from pores with different wall strength due to the relative insensitivity of accessible volume to wall strength. Finally, we note that the translational and rotational diffusivities exhibit similar qualitative behavior.

We now examine the ability of the excess entropy to describe the kinetic properties of confined dumbbells. We first focus on the sensitivity of the excess entropy scaling relations to the choice for the reference state. Figure 6 provides $D_t-s_x^{ex}$ data for $x=$f, t, and u at $T=5.0$. Recall that the goal of the excess entropy scaling strategy pursued here is to have bulk and confined fluids exhibit the same D_t-s^{ex} relationship at a given temperature. The excess entropy based upon the uncorrelated ideal gas s_u^{ex} provides the best scaling variable. $D_t-s_u^{ex}$ data for all densities, pore widths, and wall strengths considered collapse onto a common curve. The $D_t-s_f^{ex}$ and $D_t-s_t^{ex}$ correlations are noticeably weaker. From the perspective of using excess entropy scaling to predict the dynamic properties of a confined fluid, the use of s_f^{ex} or s_t^{ex} with the bulk D_t-s^{ex} relationship leads to an overestimate for the mobility of the confined fluid.

When constructing an excess entropy to describe the dynamic properties of a fluid one judiciously selects the reference state such that those correlations unimportant to a fluid's dynamic behavior are removed from the thermodynamic

entropy. By selecting s_f^{ex} as the relevant reference state entropy, one is asserting that one-body correlations do not influence a fluid's kinetic properties. The data provided in Fig. 6 suggest that these one-body correlations do indeed play an important role in establishing a confined fluid's dynamic behavior.

The excess entropy s_f^{ex} has been adopted as the relevant scaling variable in previous studies [7–13] focused on the use of excess entropy scaling strategies for describing the dynamics of confined fluids. However, as noted above, these investigations focused on systems consisting of atomistic fluids within pores defined by structureless walls, for which the difference between s_f^{ex} and s_u^{ex} is relatively small. We have now re-examined some of these systems and have found that s_u^{ex} consistently provides a superior scaling variable relative to s_f^{ex}. We again make a connection with the study of Mittal *et al.* [7], who examined the hard sphere fluid confined by smooth hard walls. For this system, $D_t - s_f^{ex}$ data for the confined fluid departed slightly from the bulk $D_t - s^{ex}$ curve at high densities, with the direction of the deviation from the bulk curve consistent with that observed in Fig. 6 (see Fig. 1 of Ref. [7]). In contrast, we find (not shown) that $D_t - s_u^{ex}$ data for the same system remain strongly correlated over the entire range of densities examined by Mittal *et al.* We plan to systematically review our earlier work in which s_f^{ex} was employed as the relevant scaling variable and report our findings in a subsequent article.

From a practical perspective the s_u^{ig} reference state has advantages over s_f^{ig}. While both quantities are connected to the fluid structure, s_u^{ig} is considerably easier to compute. Calculation of s_f^{ex} for the relatively simple diatomic molecules featured here requires evaluation of a five-dimensional integral. For molecules with more complex topologies, calculation of the one-body contribution to the ideal-gas entropy is not a trivial task [48–50]. In this case, approximate strategies are often invoked to estimate the strength of the spatial and orientational correlations that contribute to s_f^{ex}. We found the structure-based approach that was adopted here to determine s_u^{ig} to be reasonably convenient and accurate. That being said, other strategies may prove more appropriate for other systems. For example, one could deduce the accessible volume from a test-particle insertion strategy. This approach may be beneficial when working with irregularly shaped confining environments.

Figure 7 shows the $D_t - s_u^{ex}$ relationships at each of the temperatures studied here. In general, D_t and s_u^{ex} are strongly correlated. We find that, to a good approximation, the confined fluid shows the same $D_t - s_u^{ex}$ relationship as the bulk fluid at a given temperature. The picture is less clear at high density. Due to interference from the freezing transition, we are unable to obtain bulk data that extends to $-s_u^{ex}$ values as large as those characteristic of the high-density confined fluid. As a result, direct comparison of bulk and confined $D_t - s_u^{ex}$ data is not possible in this region. Further complication stems from curvature within the $D_t - s_u^{ex}$ relations at high $-s_u^{ex}$, which makes extrapolation of the curves difficult. We note that many of the confined points that deviate from the bulk curve are associated with a strong surface-fluid interaction. Some of these cases (e.g., the $H=5$ and $H=10$ points that lie well above the bulk curve at $T=2.0$) correspond to a moderate density fluid that adopts a structure with most of the particles strongly adsorbed to the pore walls and a few particles in the interior of the pore.

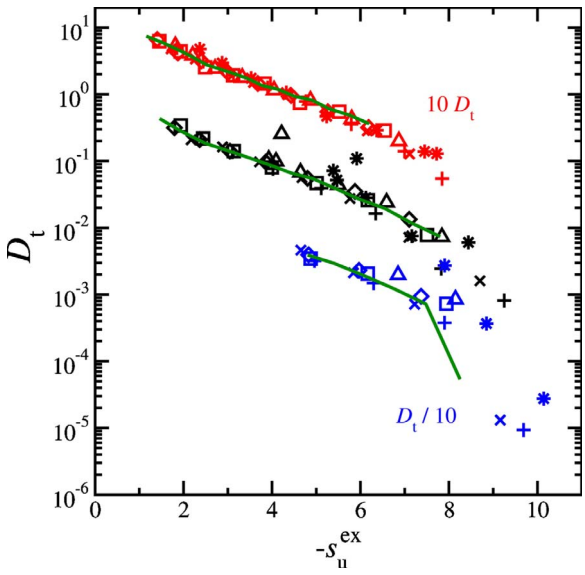

FIG. 7. (Color online) Relationship between translational diffusivity and excess entropy. Symbol shape is consistent with the definition adopted in Fig. 5. Solid lines represent the bulk fluid. Data are grouped from bottom to top as $T=1.0$ (blue), $T=2.0$ (black), and $T=5.0$ (red).

Figure 8 provides the $D_r - s_u^{ex}$, $\tau_2 - s_u^{ex}$, and $\tau - s_u^{ex}$ relationships at each of the three temperatures studied here. We again find that, to an excellent approximation, bulk and confined data for a specified dynamic property at a given temperature collapse onto a common curve when plotted against s_u^{ex}. The data presented here suggest that the change in a dynamic property upon confinement can be captured by tracking the associated variation in s_u^{ex} and referencing the bulk relationship for the dynamic property of interest and s_u^{ex}.

V. CONCLUSIONS

We have used molecular simulation to investigate issues related to the application of entropy scaling techniques to confined molecular systems. Molecular dynamics simulation was used to obtain translational and rotational diffusion coefficients, a relaxation time associated with rotational motion, and a relaxation time intended to probe the collective dynamics of the system. Free-energy-based Monte Carlo simulation methods were used to calculate thermodynamic properties of interest. Canonical Monte Carlo simulation was used to acquire one-body spatial and orientational distribution functions for the confined fluid, which are necessary for the computation of various ideal-gas configurational entropies. Properties were collected for three pore wall strengths over a range of temperatures that extends from the compressed liquid regime to the fluid regime above the critical temperature.

We found that the spatial and orientational distribution functions characterizing the structure of the confined fluid were highly localized at moderate and high fluid density. As

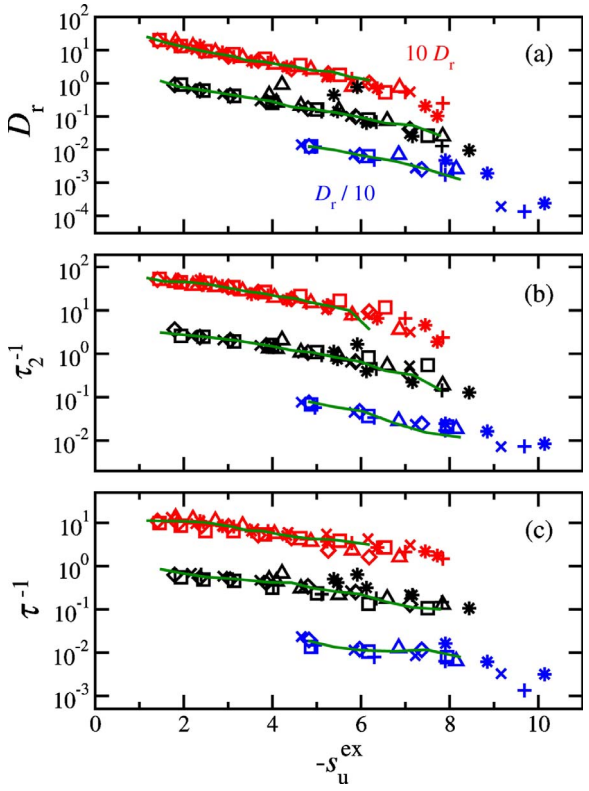

FIG. 8. (Color online) Relationship between (a) rotational diffusivity, (b) rotational relaxation time, and (c) collective relaxation time and excess entropy. Symbol shape is consistent with the definition adopted in Fig. 5. Solid lines represent the bulk fluid. Data are grouped from bottom to top as $T=1.0$ (blue), $T=2.0$ (black), and $T=5.0$ (red).

a result, one-body contributions to the ideal-gas entropy were large relative to systems that have been examined in previous studies. This aspect of the dumbbell system enabled us to carefully examine the ability of various excess entropies to describe dynamic properties. We found that the optimal reference state was that of an uncorrelated ideal gas that occupies the same volume as that accessible to the confined fluid with full interactions present. When adopting this reference state, the excess entropy accounts for one-body correlations (as well as all higher-body correlations) within the confined fluid. Our future plans include investigating the robustness of this reference state by revisiting systems that have been studied previously as well as examining new model systems that highlight differences between the states.

Our results suggest that excess entropy scaling strategies can serve as a powerful tool for describing the dynamics of confined molecular fluids. To an excellent approximation we find that the effect of confinement on the translational and rotational diffusivities as well as rotational and collective relaxation times is captured by the thermodynamic excess entropy. That being said, further studies are needed to identify the limitations of this approach. Investigations focused on molecular systems with a broader range of interparticle interactions, confining geometries, and/or compositions would be welcome. For example, we are unaware of work that has been completed with confined molecules possessing substantial intramolecular degrees of freedom and/or complex topologies.

ACKNOWLEDGMENTS

We thank Bill Krekelberg for analyzing data presented in Refs. [7,13] that helped to clarify comparisons with previous simulation studies. J.R.E. acknowledges financial support of the National Science Foundation, Grant No. CBET-0828979. T.M.T. acknowledges support from the Welch Foundation Grant No. F-1696 and from the David and Lucile Packard Foundation. Computational resources were provided in part by the University at Buffalo Center for Computational Research and the Rensselaer Polytechnic Institute Computational Center for Nanotechnology Innovations.

[1] Y. Rosenfeld, Phys. Rev. A **15**, 2545 (1977).
[2] Y. Rosenfeld, Chem. Phys. Lett. **48**, 467 (1977).
[3] R. Grover, W. G. Hoover, and B. Moran, J. Chem. Phys. **83**, 1255 (1985).
[4] Y. Rosenfeld, J. Phys.: Condens. Matter **11**, 5415 (1999).
[5] M. Dzugutov, Nature (London) **381**, 137 (1996).
[6] W. P. Krekelberg, M. J. Pond, G. Goel, V. K. Shen, J. R. Errington, and T. M. Truskett, Phys. Rev. E **80**, 061205 (2009).
[7] J. Mittal, J. R. Errington, and T. M. Truskett, Phys. Rev. Lett. **96**, 177804 (2006).
[8] J. Mittal, J. R. Errington, and T. M. Truskett, J. Chem. Phys. **126**, 244708 (2007).
[9] J. Mittal, J. R. Errington, and T. M. Truskett, J. Phys. Chem. B **111**, 10054 (2007).
[10] J. Mittal, V. K. Shen, J. R. Errington, and T. M. Truskett, J. Chem. Phys. **127**, 154513 (2007).
[11] G. Goel, W. P. Krekelberg, J. R. Errington, and T. M. Truskett, Phys. Rev. Lett. **100**, 106001 (2008).
[12] J. Mittal, T. M. Truskett, J. R. Errington, and G. Hummer, Phys. Rev. Lett. **100**, 145901 (2008).
[13] G. Goel, W. P. Krekelberg, M. J. Pond, J. Mittal, V. K. Shen, J. R. Errington, and T. M. Truskett, J. Stat. Mech.: Theory Exp. (2009) P04006.
[14] E. H. Abramson, Phys. Rev. E **76**, 051203 (2007).
[15] E. H. Abramson and H. West-Foyle, Phys. Rev. E **77**, 041202 (2008).
[16] Z. N. Gerek and J. R. Elliott, Ind. Eng. Chem. Res. **49**, 3411 (2010).
[17] T. Goel, C. N. Patra, T. Mukherjee, and C. Chakravarty, J. Chem. Phys. **129**, 164904 (2008).
[18] M. Agarwal, M. Singh, R. Sharma, M. P. Alam, and C. Chakravarty, J. Phys. Chem. B **114**, 6995 (2010).
[19] M. Agarwal and C. Chakravarty, Phys. Rev. E **79**, 030202 (2009).
[20] M. Agarwal, A. Ganguly, and C. Chakravarty, J. Phys. Chem.

B **113**, 15284 (2009).
[21] R. Chopra, T. M. Truskett, and J. R. Errington, J. Phys. Chem. B **114**, 10558 (2010).
[22] R. Chopra, T. M. Truskett, and J. R. Errington, J. Chem. Phys. **133**, 104506 (2010).
[23] J. R. Errington, T. M. Truskett, and J. Mittal, J. Chem. Phys. **125**, 244502 (2006).
[24] J. R. Errington, J. Chem. Phys. **118**, 9915 (2003).
[25] J. R. Errington, Phys. Rev. E **67**, 012102 (2003).
[26] A. P. Lyubartsev, A. A. Martsinovskii, S. V. Shevkunov, and P. N. Vorontsov-Velyaminov, J. Chem. Phys. **96**, 1776 (1992).
[27] E. M. Grzelak and J. R. Errington, Langmuir **26**, 13297 (2010).
[28] B. A. Berg and T. Neuhaus, Phys. Rev. Lett. **68**, 9 (1992).
[29] C. N. Patra and S. K. Ghosh, J. Chem. Phys. **106**, 2752 (1997).
[30] T. Lazaridis and M. Karplus, J. Chem. Phys. **105**, 4294 (1996).
[31] E. M. Grzelak and J. R. Errington, J. Chem. Phys. **128**, 014710 (2008).
[32] R. J. Speedy, F. X. Prielmeier, T. Vardag, E. W. Lang, and H. D. Ludemann, Mol. Phys. **66**, 577 (1989).
[33] D. Ben-Amotz and G. Stell, J. Phys. Chem. B **108**, 6877 (2004).
[34] C. S. Hsu, D. Chandler, and L. J. Loweden, J. Chem. Phys. **14**, 213 (1976).
[35] D. Chandler, J. D. Weeks, and H. C. Andersen, Science **220**, 787 (1983).
[36] D. Frenkel and B. Smit, *Understanding Molecular Simulation*, 2nd ed. (Academic Press, San Diego, 2002).
[37] S. Kämmerer, W. Kob, and R. Schilling, Phys. Rev. E **56**, 5450 (1997).
[38] H. J. C. Berendsen, D. van der Spoel, and R. van Drunen, Comput. Phys. Commun. **91**, 43 (1995).
[39] E. Lindahl, B. Hess, and D. van der Spoel, J. Mol. Model. **7**, 306 (2001).
[40] D. van der Spoel, E. Lindahl, B. Hess, G. Groenhof, A. E. Mark, and H. J. C. Berendsen, J. Comput. Chem. **26**, 1701 (2005).
[41] B. Hess, C. Kutzner, D. van der Spoel, and E. Lindahl, J. Chem. Theory Comput. **4**, 435 (2008).
[42] S. Nosé, Mol. Phys. **52**, 255 (1984).
[43] W. G. Hoover, Phys. Rev. A **31**, 1695 (1985).
[44] W. C. Swope, H. C. Andersen, P. H. Berens, and K. R. Wilson, J. Chem. Phys. **76**, 637 (1982).
[45] M. P. Allen and D. J. Tildesley, *Computer Simulations of Liquids* (Oxford University Press, Oxford, 1987).
[46] J. P. Ryckaert, G. Ciccotti, and H. J. C. Berendsen, J. Comput. Phys. **23**, 327 (1977).
[47] T. W. Rosch and J. R. Errington, J. Phys. Chem. B **112**, 14911 (2008).
[48] D. Chandler, J. D. McCoy, and S. J. Singer, J. Chem. Phys. **85**, 5971 (1986).
[49] D. Chandler, J. D. McCoy, and S. J. Singer, J. Chem. Phys. **85**, 5977 (1986).
[50] S. Tripathi and W. G. Chapman, J. Chem. Phys. **122**, 094506 (2005).